IEEE Access
Multidisciplinary : Rapid Review : Open Access Journal

Received May 6, 2018, accepted June 6, 2018, date of publication June 11, 2018, date of current version July 6, 2018.

Digital Object Identifier 10.1109/ACCESS.2018.2846251

Dynamic Bayesian Network-Based Approach by Integrating Sensor Deployment for Machining Process Monitoring

KANG HE[1,2], ZHUANZHE ZHAO[3,2], MINPING JIA[2], AND CONGHU LIU[4]

[1]Mine Machinery and Electronic Engineering Research Center, Suzhou University, Suzhou 234000, China
[2]School of Mechanical Engineering, Southeast University, Nanjing 211189, China
[3]School of Mechanical and Automotive Engineering, Anhui Polytechnic University, Wuhu 241000, China
[4]Sino-US Global Logistics Institute, Shanghai Jiao Tong University, Shanghai 200240, China

Corresponding author: Zhuanzhe Zhao (zhuanzhe727@ahpu.edu.cn)

This work was supported in part by the National Natural Science Foundation of China under Grant 51075070, in part by the Natural Science Foundation of Anhui Province under Grant 1808085ME127 and Grant 1708085ME104, in part by the Key Project of Natural Science Foundation of Universities of Anhui Province under Grant KJ2016A803 and Grant KJ2017A439, and in part by the Suzhou University Professor (Ph.D.) Scientific Research Foundation under Grant 2016JB09.

ABSTRACT Many condition monitoring systems based on artificial intelligence process models for machining process monitoring have been developed intensively. However, given that machining processes are very complex (i.e., nonlinear and nonstationary), there is still no clear methodology to acquire machining monitoring systems allowing machining processes to be optimized, predicted, or controlled. In this paper, the coupled hidden Markov model, based on dynamic Bayesian networks, is proposed to monitor a machining process by using multi-directional data fusion and to analyze the effect of the sensor layout on the monitoring accuracy. The features extracted by a singular spectrum and wavelet analysis constitute the input information to the system. The technique is tested and validated successfully by using two scenarios: tool wear condition monitoring (initial wear, gradual wear, or accelerated wear) for the milling process and surface roughness accuracy grade prediction (accuracy grade 9, accuracy grade 8, or accuracy grade 7) for the turning process. In the first case, the maximum recognition rate obtained by the single-sensor placement for tool wear is 83%, whereas in the case of the three-sensor placement, the model recognition rate is 89%. In the second application for turning, the maximum recognition rate obtained by the single-sensor and the double-sensor placements for surface roughness accuracy prediction is 77% and 85%, respectively. In the case of the three-sensor placement, the model recognition rate is 89%. The proposed approach can also be integrated into the diagnosis architecture for condition monitoring in other complex machining systems.

INDEX TERMS Condition monitoring, dynamic Bayesian network, coupled hidden Markov model, sensor deployment, machining process.

I. INTRODUCTION

Machining process monitoring (MPM) is crucial for reducing cost, ensuring greater product variability, and improving manufacturing productivity and reliability [1]. An efficient condition monitoring scheme is capable of providing warnings for dimension tolerance (i.e., surface roughness deterioration) and predicting machine parts failure (i.e., tool breakage) at the early stages. Therefore, MPM is the measurement and estimation of certain key process variables [1]. Given the advantage of direct measurement, some critical process variables are gauged directly [2]. However, many process variables cannot be directly measured because of the complexity of the machining processes (i.e., nonlinear, nonstationary, etc.), Moreover, the high cost of the measurement devices and their sophisticated designs do make them unsuitable for real-time industrial applications [3]. Therefore, the strategy has to be developed on the basis of indirect measures and evaluations.

The development of sensors and sensing techniques has made it possible to monitor and control the machining process. Research issues related to the monitoring of machining systems are mainly based on artificial intelligence (AI) process models. As a data-based process monitoring [4], AI has become a key technology in process industries.

Compared with the other existing learning algorithms [5]–[7], the strategy of AI process models has higher accuracy, usefulness and versatile for surface roughness prediction and tool condition monitoring. Furthermore, as a data mining and analytics approach [8], several status signals (the device itself and the process signals) are proposed to be considered as the model input. Thus the strategy of multi-sensor fusion was introduced to achieve an ideal and reliable prediction. However, little information is available in the literatures about how to perform this task [9], [10]. As a sensor fusion model, an artificial neural network (ANN) has been a popular means for machining process monitoring [11]. ANN with seven inputs, including the tool insert grade, the workpiece material, the cutting force, and the vibration acceleration, are used to predict the surface roughness in turning [12]. Literature demonstrates that, with the same fusion data input, ANN provides better results than multiple regression [13]. The prediction accuracy of ANN is affected by the network architecture and the activation functions. However, thus far, no exact solution has been obtained [14]. Although ANN has been widely used for its learning and adaptive capacity in MPM, adequate training sets are needed in the modeling and the convergence generally takes a long time. Moreover, the fixed-length input sequence makes it impossible to determine the optimal length required to improve the recognition rate and shorten the training time [8], [15]. Given the randomness and uncertainties in the machining process, compared with ANN, stochastic approaches, such as the Bayesian network (BN), have proven to be effective and accurate in modeling both dynamic and static signals [16]. Some literatures demonstrate the superiority of Bayesian networks over ANNs on the efficacy of surface roughness prediction in high-speed machining [17]. Furthermore, the capacity of coping with missing values as well as multi-source data fusion stands it out among other traditional techniques for monitoring large-scale plant-wide processes [18], [19]. However, as a multi-sensor fusion model, BN has been less widely used. TABLE 1 summarizes these sensor fusion systems applied in machining process monitoring.

Apart from the multi-sensor fusion model, sensor signal feature selection is still a critical component. Signals applied in MPM are generally cutting-force signals, vibration signals, current or power signals, and acoustic emission signals. The application of these signal features was discussed in the time domain, frequency domain, and wavelet domain by Abellan-Nebot [48]. A detained statistical analysis of 35 relevant papers revealed that most of the features are mainly concentrated in the time domain, more common in the case of the mean, followed by the frequency domain, more common in the case of the single harmonic. Notably, in the wavelet domain, fewer features are extracted. The descriptors are shown in FIGURE 1. In addition to the limitations related to the feature selection, most of the existing monitoring systems are application-specific; i.e., they focus on either tool condition monitoring (TCM) or dimensional accuracy prediction, but not on both.

Whether BN or ANN has to be used as a fusion model needs to be determined to use a multi-sensor system. Sensors and sensing technologies constitute the fundamental basis for MPM in that the performance of a supervising system critically depends on the accuracy and efficiency of sensor measurements in the case of faulty symptoms. The capability of sensor measurements in the case of faulty signatures, using force sensors, vibration sensors, or AE sensors, is subject to the influence of the measuring points [48]. The multi-sensor strategy was widely adopted in many previous studies [12], [16], [46], [48]. However, no further study has been conducted to analyze the effect of the sensor deployment on the monitoring system's capability. Although many studies have shown that the sensitivity of information obtained by sensors in different directions is different to the process variables [49]–[51], the effect of multi-directional data coupling on the key process variables remains to be further studied.

From the above literature review, we identified that when developing a system for MPM, the current literature lacks sufficient consideration of the following issues related to feature selection and modeling:

(1) As can be seen from TABLE 1, with respect to a multi-sensor fusion model, the application of BN in the field of machining process monitoring has been very limited. Therefore, BN-based machining process monitoring needs to be further explored.

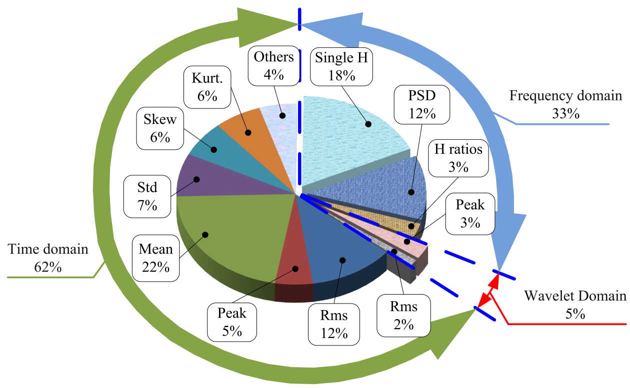

FIGURE 1. **Feature descriptors applied in MPM.**

(2) As can be seen from FIGURE 1, most of the features used in the previous studies are mainly concentrated in the time domain and the frequency domain. While in the wavelet domain, fewer features are extracted. A previous study by Zhu *et al.* [52] showed that the wavelet-based feature extraction method is a powerful tool for TCM.

(3) Because the status information picked up by sensors in different measurement locations is significantly different to the process variables, it is necessary to analyze the effect of the sensor layout on the system capacity for MPM. However, this has been rarely studied thus far.

(4) Most of the existing monitoring systems are application-specific, either for a tool wear diagnosis or for a dimensional accuracy prediction. The application of the

TABLE 1. Sensor fusion systems applied in machining processes.

Sensor Type	Fusion Models	Application object	Ref.
Accelerometer, Dynamometer	BN	Tool wear diagnosis	[20]
Fiber Bragg grating sensor	BN	Tool wear diagnosis	[21]
Accelerometer	BN	Tool wear diagnosis	[22]
Dynamometer	BN	Tool wear diagnosis	[23, 24]
Accelerometer, AE	NN	Tool wear diagnosis	[25]
Dynamometer	NN	Tool wear diagnosis	[26, 27]
Vision system	NN	Tool wear diagnosis	[28-30]
Dynamometer, accelerometer	NN	Tool wear diagnosis	[31]
Vision system	NN	Tool breakage detection	[32]
Current sensor	NN	Tool wear diagnosis	[33]
Laser Doppler vibrometer	NN	Surface roughness prediction	[34]
Dynamometer	NN	Surface roughness prediction	[35]
Accelerometer, vision system	NN	Surface roughness prediction	[36, 37]
Accelerometer	NN	Surface roughness prediction	[38, 39]
Accelerometer, current sensor	NN	Tool wear diagnosis	[40]
Accelerometer	NN	Tool wear diagnosis	[41]
Dynamometer, accelerometer	NN	Tool wear diagnosis	[42]
Microphone	NN	Tool wear diagnosis	[43]
Dynamometer, accelerometer	NN	Surface roughness prediction and dimensional deviation	[44] [45]
Dynamometer, accelerometer, spindle current, voltage sensor, sound pressure level	NN	Tool wear diagnosis	[46, 47]

feature extraction and multi-sensor fusion model to different machining systems needs to be explored further.

In the present study, we considered these four issues as the research questions, which will be solved in the following sections.

II. FEATURE DESCRIPTION AND GENERATION

Tool-tip vibration displacements in three directions were observed during the turning process. Taking into account the cutting-plane strain, an orthogonal cutting simulation was performed to reveal the microscopic tool-tip displacement state based on Deform-3D. Assume that the tool was made of elastomers; then, by setting the tool boundary displacement conditions, a WC-based tool was adopted to cut the die steel H13(cutting speed $Vc = 120$ m/min, feed $f = 0.05$ mm/r, depth of cut $ap = 0.1$ mm). The deformation displacement of the tool tip is shown in FIGURE 2. The maximum displacement of the tool tip in the tangential direction (y), radial direction (x), and axial direction (z) was 1.73 *mm*, 0.145 *mm*, and 0.162 *mm*, respectively. Three enlarged views on the right side show the effect of the tool-tip vibration displacement on the workpiece surface topography. Along the tangential direction (y) (above), the tool-tip vibration displacement (ε_y) affected by the elastic recovery damping of the workpiece [53] led to the changes in ε'_x in the radial direction (x), which affected the depth of the cut in the turning process. Along the radial direction (x) and the axial direction (z), it essentially changed the intersection of the two adjacent corner radii mapped on the workpiece surface. When the axial direction (z) was considered an example, the point p was the intersection of the ideal profile (without any tool-tip vibration) shown by the solid lines, wherein the mean line was *oo'*. The actual profile drawn with broken lines deviated from the ideal profile with the maximum value of ε (ε_x and ε_z), which led from the point p to the position p'. The overlap affected the calculation of the mean line, i.e., the ratio of h_{0+}/h_0 changed to h_{1+}/h_{1-}, which led to the change in the surface roughness. The same was observed in the case of the radial direction (x). Thus, the tool-tip vibration in three directions had a direct effect on the surface roughness. Therefore, the vibrational data fusion in three directions more fully reflected the dynamic changes in the surface roughness.

Different from single-point turning, milling was mainly involved in the multi-tooth continuous cutting. During the milling process, the cutting forces and torques were periodic. This was attributed to the cutter geometry, the geometric angles installed, and the operation itself [54]. During one rotation of a milling cutter, each tooth entered, moved through, and then, exited the workpiece. Each of these cutters was affected by the cutter wear and change in the cutting force. FIGURE 3 shows the tool wear and force situation of a single blade during the milling process. According to the residual stress analysis, the cutting force F was the resultant force of the radial force F_y and the normal force F_n. The radial force F_y was mainly affected by the shear force and the friction between the tool flank and the workpiece. When the chip thickness was constant, the flank wear V_B was the main influence on F_y. When the tool flank wore

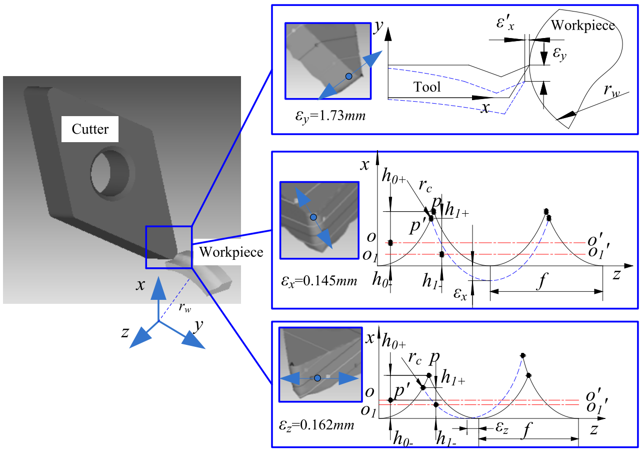

FIGURE 2. Effect of tool-tip vibration on the workpiece surface topography.

down, the small facet (relief angle $\alpha' = 0°$) was formed on the flank surface. As the flank wear increased gradually, the small facet increased, in turn increasing the contact area between the tool flank and the workpiece. Thus, the radial forces F_y increased. The normal force F_n was determined using not only the friction between the rake face and the chip but also the effect of the flank face and the workpiece-generated extrusion. Zhao *et al.* [55] studied the effect of some parameters, such as the flank face's normal stress σ, tool hardness H_B, tool clearance α, chip width W_d, cutting speed V_c, and tool flank wear V_B, on the basis of the normal force F_n and formulated the following equation:

$$V_B = K \cdot \left(\frac{2V_c \cdot t}{W_d^2 \cdot H_B \cdot tg\alpha}\right)^{\frac{1}{3}} \cdot \sqrt[3]{F_n} \tag{1}$$

where K is a coefficient determined experimentally. As can be seen from Eq. (1), with the other parameters unaltered (e.g., cutting length $L = V_c \cdot t$), the normal force F_n will be affected by the tool flank wear V_B. As can also be seen from Fig. 3, the resultant force and the normal force can be expressed as follows:

$$F_x = F_n \cdot \sin\kappa_r \tag{2}$$

$$F_z = F_n \cdot \cos\kappa_r \tag{3}$$

where κ_r is the tool's main angle. Thus, the tool's flank wear V_B was reflected by the triaxial force (F_x, F_y, and F_z) to some degree. Therefore, the data fusion of the triaxial force for TCM was relatively advantageous.

Feature generation was achieved using the singular spectrum analysis (SSA) [56] and the wavelet multi-resolution analysis (WMA). Let $\{y_t | t = 0, 1, \cdots, N-1\}$ be a time series of length N, let L be the length of the sliding window, and set $K = N - L + 1$. The trajectory matrix $H = (H_1, H_2, \cdots, H_K)$, where $H_j = (y_{j-1}, y_j, \cdots, y_{j+L-2})^{\mathrm{T}} \in \mathbb{R}^{\mathrm{L}}$ and $j = 1, 2, \cdots, K$ are the L-lagged vectors. Let $\mathcal{S} = H \times H^{\mathrm{T}}$; the matrix H is then subjected to a singular value decomposition and can be expressed as $H = \sum_{i=1}^{d} E_i$, where E_i are the rank-one elementary matrices and d is the number of non-zero eigenvalues of $\mathcal{S}$. Let the j-th principal component be p^j; the $p_i^j = \sum_{k=i-1}^{L+i-2} \psi_k u_{k-i+2}^j$. Let $\Psi = \left\{\left\{\psi_i^j \mid 1 \le i \le N, 1 \le j \le L\right\}\right\}$ be a reconstruction set of a time series; therefore, the entries of ψ can be estimated as follows:

$$\psi_{i-1}^j = \frac{1}{L}\sum\nolimits_{m=1}^{i} u_m^j p_{i-m+1}^j \tag{4}$$

Ψ corresponded to the different principal components and features bands. However, these spectral components were not completely independent in that SSA was based on the singular value decomposition of H rather than the spectrum segmentation [56]. To further decompose the time series Ψ, the MRA of the wavelet was adopted. Let $\{V_j, j \in Z\}$ be a closed subspace of $L^2(R)$; then, W_j was the complement space between V_j and V_{j-1}, and thus, $V_0 = V_M \oplus \bigcup_{j=1}^{M} W_j$. Therefore, Ψ can be an orthogonal decomposition by a db4 wavelet using five-layer wavelet decomposition, expressed as follows:

$$\psi^k(t) = \sum\nolimits_{i=-\infty}^{M} \sum\nolimits_{-\infty}^{+\infty} a_{i,j}\phi_{i,j}(t) + \sum\nolimits_{j=-\infty}^{+\infty} b_{i,j}\varphi_{i,j}(t) \tag{5}$$

where M is the decomposition level, $a_{i,j}$ are the wavelet coefficients, and $b_{i,j}$ are the i^{th} layer scale decomposition coefficients. The feature E_R used for the supervising machining process was denoted as follows:

$$E_R = \frac{\|A_R\|^2}{\sum_R \left(\|A_R\|^2 + \|B_R\|^2\right)} \tag{6}$$

where $||\cdot||$ denotes the norm, $R \in \{x, y, z\}$ is the tool vibration direction, $A_R = \{a_{i,j}\}$, and $B_R = \{d_{i,j}\}$, where $1 \le i, j \le M$.

III. MACHINING PROCESS MONITORING USING DBN

As an extension of Bayes nets (BNs), DBN is a powerful sequence data simulation tool, typically used to model probability distributions over semi-infinite collections of random variables, $Z_1, Z_2, \cdots, Z_{\mathrm{p}}$. Assume that the observation

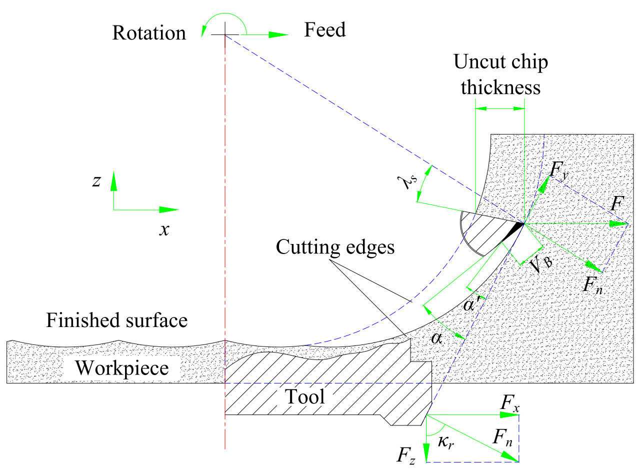

FIGURE 3. Schematic illustration of milling process.

$o_t = \left(o_t^1, o_t^2, \cdots, o_t^L\right) \in O^{\otimes L}$ and its corresponding hidden state $q_t = \left(q_t^1, q_t^2, \cdots, q_t^L\right) \in Q^{\otimes L}$ was a Markov chain. In HMM, $Z_t = \{o_t, q_t\}$, and its state space consisted of a single random variable $q_t(L = 1)$, but a DBN represented the hidden state in terms of a set of random variables $q_t(L > 1)$. The major benefit of HMM represented by DBN was that a DBN had a more general graph structure form and was used to express more complex topology than HMM. Further, the flexible algorithms of the DBN were adopted to quicken the rate of reasoning.

As can be seen from the analysis of the tool vibration during the turning process and the cutting force in the milling process mentioned above, the multi-directional data were a more comprehensive description of the surface morphology formation and the tool wear progressive course [53]. As the single-state sequence structure limited its ability to model multi-directional data, HMM was not suitable for multi-directional data fusion. Therefore, a DBN model-coupled hidden Markov model (CHMM) was proposed for use as a multi-directional data fusion model for MPM. An example of a CHMM_r represented by a DBN is shown in FIGURE 4. As discussed earlier, assume that o_t was the observation at time t, $o_t = \left(o_t^1, o_t^2, \cdots, o_t^L\right) \in O^{\otimes L}$, and q_t was the hidden state at time t, $q_t = \left(q_t^1, q_t^2, \cdots, q_t^L\right) \in Q^{\otimes L}$, where $1 \le t \le T$; then, a CHMM with L chains was characterized using the following elements:

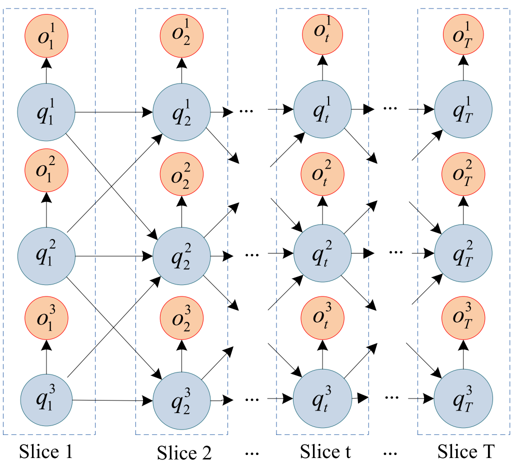

FIGURE 4. CHMM_*r* represented by a DBN.

(1) Initial state distribution π, where $\pi = \left\{\pi_i^l\right\} = \left\{P\left(q_1^l = S_i^l\right)\right\}, \sum_{i=1}^N \pi_i^l = 1, 1 \le l \le L, 1 \le i \le N$, N is the number of hidden variables of each chain.

(2) Observation symbol probability distribution in state j, $B = \left\{b_j^l(m)\right\}$, where $B = \left\{P\left(o_t^l = v_m^l | q_t^l = S_j^l\right)\right\}, \sum_{i=1}^M b_j^l(m) = 1, 1 \le l \le L, 1 \le j \le N, 1 \le m \le M$.

(3) State transition probability distribution $\boldsymbol{A}$, where $A = \left\{a_{ij}^l\right\} = \left\{P\left(q_{t+1}^{l'} = S_j^{l'} | q_t^l = S_i^l\right)\right\}, \sum_{j=1}^L a_{ij}^l = 1, 1 \le l, l, \le L, 1 \le i, j \le N$.

For the sake of convenience, a CHMM can be represented by using a compact notation as follows: $\boldsymbol{\lambda} = (\boldsymbol{\pi}, \boldsymbol{A}, \boldsymbol{B})$. On the basis of the forward and backward variables of HMM, the forward operator α and the backward operator β of the CHMM can be defined as follows: $\alpha_t(i) = P\left(o_1, o_2, \cdots, o_t, q_t^1 = S_i^1, q_t^2 = S_i^2, \cdots, q_t^L = S_i^L | \lambda\right), \beta_t(i) = P\left(o_{t+1}, o_{t+2}, \cdots, o_T | q_t^1 = S_i^1, q_t^2 = S_i^2, \cdots, q_t^L = S_i^L | \lambda\right)$, where $i = \left(i^1, i^2, \cdots, i^L\right), o_\tau = \left(o_\tau^1, o_\tau^2, \cdots, o_\tau^L\right), 1 \le \tau \le T$. The recursive procedure for estimating α and β can be stated as follows:

$$\alpha_t(i) = \begin{cases} \prod_{l=1}^L \pi_i^\ell b_i^\ell\left(o_1^\ell\right), & t = 1 \\ \sum_{i'=i^1}^{i^l}\left[\alpha_{t-1}(i') a_{i',i} \prod_{l=1}^L b_i^\ell\left(o_t^\ell\right)\right], & \\ \quad t = 2, 3, \cdots, T \end{cases} \tag{7}$$

$$\beta_t(i) = \begin{cases} 1, & t = T \\ \sum_{i'=i^1}^{i^l}\left[a_{i,i'} \prod_{l=1}^L b_{i'}^\ell\left(o_{t+1}^\ell\right) \beta_{t+1}(i')\right], & \\ \quad t = T-1, T-2, \cdots, 1 \end{cases} \tag{8}$$

The CHMM parameter learning was implemented using the EM algorithm. That is, it had to maximize. $\Theta\left(\lambda, \hat{\lambda}\right) = E\left|\log P\left(O, Q|\hat{\lambda}\right)\right| O, \lambda|$. Because the current state depended only on the previous state, we obtained the following:

$$\begin{aligned} &\Theta\left(\lambda, \hat{\lambda}\right) \\ &\quad = \sum_{q \in Q} P(O, Q|\lambda) \log\left(P\left(O, Q|\hat{\lambda}\right)\right) \\ &\quad = \sum_{q \in Q} P(O, Q|\lambda) \log \pi_{q_1}^l + \sum_{q \in Q}\sum_{t=2}^T P(O, Q|\lambda) \log a_{q_{t-1}, q_t}^l \\ &\qquad + \sum_{q \in Q}\sum_{t=1}^T P(O, Q|\lambda) \log\left(b_{q_t}^l(o_t)\right) \end{aligned} \tag{9}$$

Obviously, Eq. (9) consists of three terms, which can be used to train different CHMM parameters. By using the Gibbs inequality [57], we obtained the final update formula as follows:

$$\hat{\pi}_i^l = \frac{\alpha_1(i)\beta_1(i)}{\sum_{j=1}^N \alpha_1(j)\beta_1(j)}, \quad 1 \le l \le L \tag{10}$$

$$\hat{b}_j^l(m) = \frac{\sum_{t=1}^{T-1}\sum_{i=1}^N \xi_t^l(i,j)|_{o_t = v_m}}{\sum_{t=1}^T \sum_{i=1}^N \xi_t^l(i,j)}, \quad 1 \le m \le M \tag{11}$$

$$\hat{a}_{i,j}^l = \frac{\sum_{t=1}^{T-1}\xi_t^l(i,j)}{\sum_{t=1}^{T-1}\sum_{j=1}^N \xi_t^l(i,j)}, \quad 1 \le i, j \le N \tag{12}$$

where $\xi_t^l(i,j)$ is the probability of being in state S_i^l at time t, and in state $S_j^{l'}$, at time $t+1$, $\xi_t^l(i,j) = P\left(q_t^l = S_i^l, q_{t+1}^{l'} = S_j^{l'} | O, \lambda\right), 1 \le l, l' \le L$.

On the basis of the accuracy grade of Ra defined by GB/T1031-2009 and the tool wear progressive change, both surface roughness prediction and tool condition monitoring could be converted into a pattern classification problem. As DBN training is not suitable for a single-state model, for the monitoring of the machining process, the following criterion was used:

Definition: Consider an observation sequence $O = \{O^{(1)}, O^{(2)}, \cdots, O^{(k)}, \cdots, O^{(K)}\}$, where $O^{(k)}$, $1 \leq k \leq K$, is the k^{th} observation sequence. Assume LP to be the logarithmic probability of the observation sequence $O^{(k)}$ corresponding to the state S_j. As the training sets of each state overlapped with each other, which was analogous to the penetration among the states, the state infiltration rate (SIR) was defined as follows:

$$SIR(k,j) = \frac{LP_j(k)}{\sum_{i=1}^{N} |LP_i(k)|}, \quad 1 \leq k \leq K, \ 1 \leq j \leq N. \tag{13}$$

where. $LP_j(k) = \sum_Q \left(logP\left(O^{(k)}, Q|\lambda_j\right)\right)$, $1 \leq i \leq m, 1 \leq j \leq N$ Then, the state that the k^{th} observation sequence belonged to was given by. $j_k^* = arg\ \max_{1 \leq j \leq N} \{SIR(k,j)\}, 1 \leq k \leq K$.

In general, either random or uniform initial estimates of the $\{\pi_i, a_{ij}\}$ are adequate for obtaining useful re-estimates in almost all cases. However, for $\{b_j(o_t)\}$, good initial estimates were helpful only in the discrete symbol case. Firstly, $\{b_j(o_t)\}$ was randomly initialized; then, the optimal state sequence was determined by using the Viterbi algorithm. Therefore, $\{b_j(o_t)\}$ was calculated as follows:

$$\hat{b}_j(k) = \frac{\text{Expected number of times in state } j \text{ and observing symbol} v_k}{\text{Expected number of times in state } j} \tag{14}$$

As mentioned earlier, because of the non-stationary signals and the diversity of the training samples, the strategy that all the training samples be involved in modeling was not the best choice. Therefore, a second-order feature selection method based on the shuffled frog leaping algorithm (SFLA) [58] was developed. The entire procedure was as follows:

(1) In the feasible space R^D, determine the number of samples p used for building a single model. The entire collection of the states generated F frogs to form the initial population $U \subset R^D$.

(2) Assuming that the i^{th} frog was $U_i = \left\{U_{r,k}^i\right\}_{k=1}^D \in U, 1 \leq r \leq p$, based on the Fisher linear discriminant analysis [59], the feature selection was performed by comparing the class spacing between the samples. Denoting the mathematical expectation of the r^{th} sample of the i^{th} frog as $E\left\{U_{r,k}^i\right\}$, the r^{th} sample of the j^{th} frog as $E\left\{U_{r,k}^j\right\}$, $i \neq j$, and the main diagonal elements of the covariance matrix of the i^{th} and the j^{th} frogs as C_r, we defined the fitness function as follows:

$$f(i,j) = \frac{\sum_{i=1}^{N}\left[E\left\{U_{r,k}^i\right\} - E\left\{U_{r,k}^j\right\}\right]\left[E\left\{U_{r,k}^i\right\} - E\left\{U_{r,k}^j\right\}\right]^T}{\sum_{r=1}^{p} C_r} \tag{15}$$

Where $1 \leq i \leq M, 1 \leq j \leq N$. The fitness value of the frog pair $\{U_i, U_j\}$ could be calculated according to Eq. (15).

(3) Set $j+1 \rightarrow j$; step (2) was executed repeatedly until $j > N$. Sort the f values in the order of decreasing performance value: $f(U_i) = \left\{f_i^1, f_i^2, \cdots, f_i^j, \cdots, f_i^N\right\}$.

(4) Set $i+1 \rightarrow i$, the step (2) and step (3) are executed repeatedly until $i > M$. Sort the f in order of decreasing performance value. $f_F = \left\{f(U_1), f(U_2), \cdots, f(U_i), \cdots, f(U_M)\right\}$.

(5) U_k was the feature set selected, where. $k = arg\ max_{1 \leq i \leq M} \{f(U_i)\}$.

Condition monitoring in a machining process is concerned chiefly with sensor selection, feature selection/extraction, and the selection of an appropriate classification model. The basic framework of condition monitoring in a machining process is illustrated in FIGURE 5.

IV. CASE STUDY

To illustrate the proposed condition monitoring approach in the machining process, two case studies, one for tool wear condition monitoring in high-speed milling and the other for surface roughness accuracy grade prediction in the turning process, were developed.

A. APPLICATION TO TOOL CONDITION MONITORING IN HIGH-SPEED MILLING

1) MATERIAL AND EQUIPMENT

The tool condition monitoring method presented in the previous section was tested on the ''prognostic data challenge 2010'' database [60]. A high-speed CNC machine (Röders Tech RFM760) with three-flute cutters and a spindle speed of up to 42000 *rpm* was selected for the experiment. The workpiece material was stainless steel (*HRC*52). The cutting parameters were as follows: the spindle speed of the cutter was 10400*rpm*, the feed rate was 1555 *mm/min*, the *y* depth of the cut (radial) was 0.125*mm*, and the *z* depth of the cut (axial) was 0.2 *mm*. The data were recorded using a dynamometer, accelerometer, and an acoustic sensor during the cut process, and the amount of wear was measured after each cut. The data were acquired at 50 *k*Hz/channel. Given the advantage of the cutting force that best describes the tool wear progress [40], [42], the cutting force was used in this study. FIGURE 6 illustrates the test bed. A Kistler quartz three-component dynamometer was mounted between the workpiece and the machining table to measure the cutting forces. For simulation purposes (learning and online wear estimation), 78 samples were selected from Cutters 1 and 6

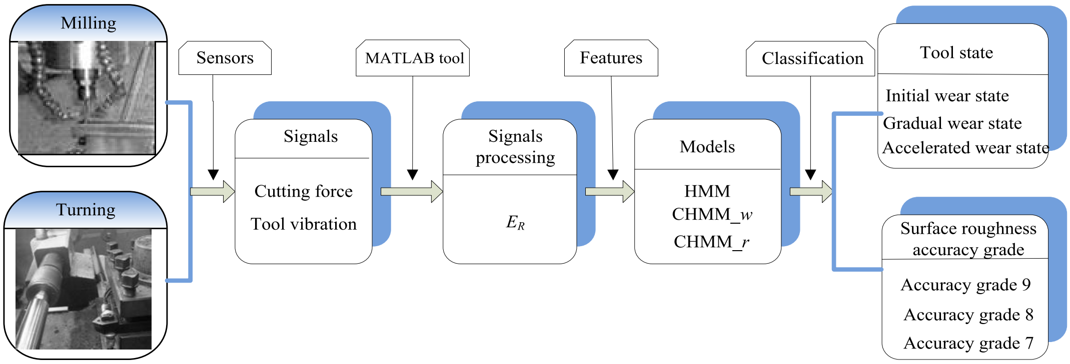

FIGURE 5. Framework of machining process monitoring.

TABLE 2. Extraction features and tool wear value.

No of cuts	Cutter 1							Cutter 6						
	V_B (μm)	E_R			Code			V_B (μm)	E_R			Code		
		S_x	S_y	S_z	C_x	C_y	C_z		S_x	S_y	S_z	C_x	C_y	C_z
1	29.1020	0.494	0.425	0.466	20	25	21	39.6435	0.509	0.445	0.460	19	21	21
2	56.6255	0.501	0.455	0.465	20	21	21	47.4438	0.498	0.457	0.469	20	21	21
3	63.9914	0.498	0.446	0.452	20	21	21	54.1895	0.507	0.460	0.472	15	21	21
4	71.4248	0.511	0.447	0.453	20	21	21	60.0007	0.501	0.449	0.468	20	21	21
5	74.9464	0.500	0.452	0.431	15	21	21	64.9862	0.508	0.457	0.462	19	21	21
6	78.0603	0.499	0.443	0.443	20	21	22	69.2439	0.494	0.455	0.460	20	21	21
7	80.1685	0.511	0.449	0.444	20	16	21	72.8623	0.500	0.449	0.449	20	21	17
8	82.3157	0.496	0.434	0.455	20	17	13	75.9424	0.499	0.446	0.457	20	21	21
…	…	…	…	…	…	…	…	…	…	…	…	…	…	…
74	201.8819	0.628	0.406	0.423	9	17	5	153.0461	0.589	0.405	0.416	9	20	4
75	204.848	0.568	0.411	0.418	9	13	4	155.0774	0.647	0.399	0.399	2	20	5
76	207.7751	0.596	0.412	0.431	13	17	5	157.1811	0.636	0.394	0.405	2	20	5
77	210.5553	0.539	0.421	0.461	9	12	4	159.3614	0.574	0.407	0.406	9	20	4
78	213.0449	0.510	0.428	0.456	13	21	4	161.6223	0.592	0.397	0.404	9	20	5

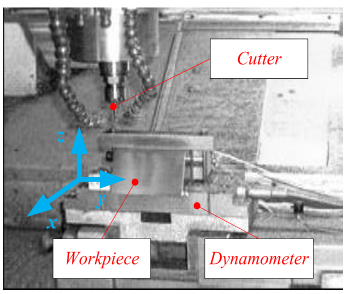

FIGURE 6. TCM in high-speed milling [60].

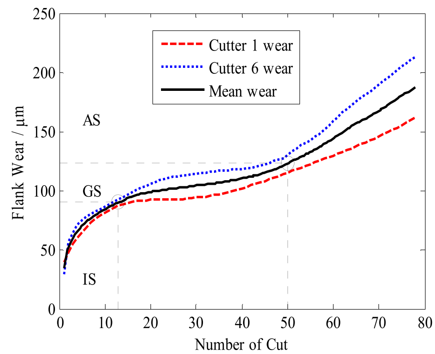

FIGURE 7. Tool wear fitted by B-spline interpolation.

at regular intervals (Cutter 1 for learning and Cutter 6 for testing).

We took the average of the three-flute flank wear values V_B, $V_B = 1/3(V_{B1} + V_{B2} + V_{B3})$ as the final flank wear value. The flank wear progressive change was approximated by using a B-spline curve and the tool states (initial wear state: $IS \leq 90\ \mu m$; gradual wear state: $90\ \mu m < GS \leq 123\ \mu m$; accelerated wear state: $AS > 123\ \mu m$) were determined by using the crossover points of the second-order derivative of the fitted flank wear curve (FIGURE 7). The feature E_R was extracted and then encoded using a 5×5 codebook based on SOM. TABLE 2 shows the features extracted and the corresponding tool wear values.

Based on the analysis of the tool degradation curves, three wear stages were defined to classify the different features in the different wear stages. FIGURE 8 shows the number of cuts in Cutter 1 and Cutter 6 for the three tool wear stages.

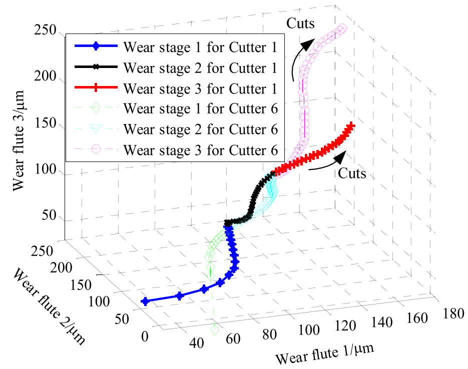

FIGURE 8. **Wear conditions for Cutter 1 and Cutter 6.**

For example, for Cutter 1, the features from the first 15 cuts belonged to *IS*; then, the next 40 cuts were classified in *GS*, and the last 23 cuts in *AS*. For the HMM, both the initial state probability vector $\boldsymbol{\pi}$ and the state transition probability matrix $\boldsymbol{A}$ were randomly initialized, and the observation symbol probability matrix $\boldsymbol{B}$ was estimated according to Eq. (14). For example, the π and $\boldsymbol{A}$ of the HMM were initialized as follows:

$$\pi = \begin{bmatrix} 0.0320 \\ 0.0227 \\ 0.2236 \\ 0.3282 \\ 0.3935 \end{bmatrix},$$

$$A = \begin{bmatrix} 0.0599 & 0.0747 & 0.2774 & 0.2076 & 0.3805 \\ 0.2530 & 0.3533 & 0.1170 & 0.0373 & 0.2395 \\ 0.1765 & 0.1170 & 0.2459 & 0.0861 & 0.3745 \\ 0.0054 & 0.2380 & 0.3103 & 0.4112 & 0.0352 \\ 0.1862 & 0.0897 & 0.4053 & 0.0825 & 0.2398 \end{bmatrix}$$

For the CHMM_*r*, $\boldsymbol{\pi}$ and $\boldsymbol{A}$ were randomly initialized. For the $\boldsymbol{B}$ parameters, each chain of CHMM_*r* was initialized individually by using Eq. (14), and then, the results of each chain were regarded as the initial value of $\boldsymbol{B}$. The structural parameters of each model are selected, as shown in TABLE 3.

TABLE 3. **Model structure parameters.**

Model	Sensor	Model structure			
		Markov chain type	Number of states	Coding range	Inference engine
HMM	*Sz*	Ergodic	5	1~25	Forward-Backward Algorithm
	Sx	Ergodic	5	1~25	Forward-Backward Algorithm
	Sy	Ergodic	5	1~25	Forward-Backward Algorithm
CHMM_*r*	*Sx* ,*Sy*, *Sz*	Ergodic	5×5×5	1~25	jtree_dbn

To avoid the sample skew, in base *IS*, the samples of Cutter 1 were divided into five training sets denoted as *IS*, *GS*, *GS*, *AS*, and *AS*. Obviously, if *GS* was chosen for λ_{GS} learning, the samples of *GS* in the vicinity of the border between *IS* and *GS* was misjudged as *IS*. Therefore, the selection *GS* for λ_{GS} learning was inappropriate. The same was true for the selection of *AS*. Therefore, *IS*, *GS*, and *AS* were adopted for training HMM and CHMM_*r*.

2) RESULTS AND DISCUSSION

To simulate an online monitoring process, *SIR* calculated with CHMM_*r* was plotted with respect to the test samples of Cutter 6. FIGURES 9∼11 show the test results. One can see in FIGURE 10 that the misjudged samples are mainly concentrated in the vicinity of the border between *IS* and *GS*. To quantify the system monitoring accuracy, the recognition rate is defined as follows:

$$C_R = \frac{\textit{Correctly classified samples}}{\textit{Correctly classified samples} + \textit{Misclassified samples}} \times 100\% \tag{16}$$

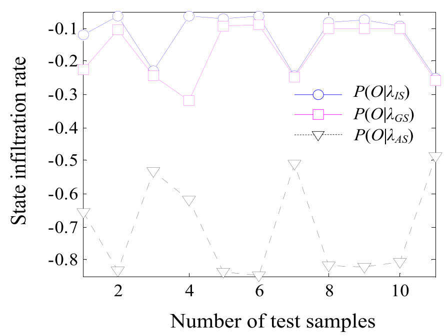

FIGURE 9. ***SIR*** **for** ***IS*** **samples.**

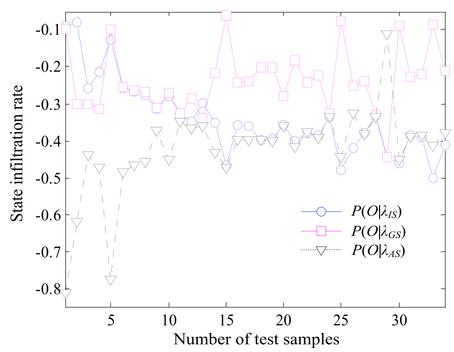

FIGURE 10. ***SIR*** **for** ***GS*** **samples.**

TABLE 4 shows the results obtained using the HMM and CHMM_*r* approaches. We found that the recognition rate changed considerably when we used data from a single direction, which were 50%, 75%, and 83% using the sensor in the *z*, *x*, and *y* direction, respectively. The possible

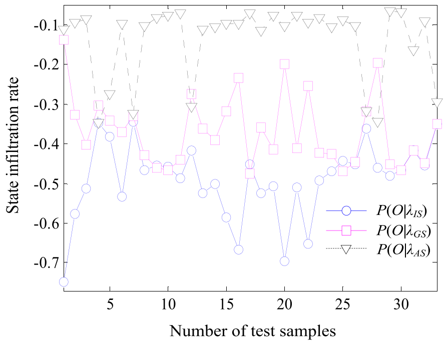

FIGURE 11. ***SIR*** **for** ***AS*** **samples.**

TABLE 4. **Classification results of tool wear states.**

Approachs	Orientation	Sensor group	Sample size	C_R
HMM	*z* dir.	{ *Sz* }	78	50%
	x dir.	{ *Sx* }	78	75%
	y dir.	{ *Sy* }	78	83%
CHMM_*r*	*x* dir., *y* dir., *z* dir.	{ *Sx* ,*Sy*, *Sz* }	78	89%

reasons were as follows: The cutting force signals in the three directions might be seen as the output responses of a multi-input system in the$x$, y, and z directions. As the cutting directions of the piezoelectric material (e.g., quartz crystal) in the triaxial force sensor were different, the sensitivity of the piezoelectric material being subjected to the force was not the same in each direction. Moreover, FIGURE 3 shows that when the chip thickness was constant, the radial force F_y was mainly affected by the tool's flank wear *VB*. Therefore, F_y was more sensitive to the tool's flank wear [37]. Further, Eqs. (2) and (3) show that the feed force F_x and the axial force F_z were mainly determined by the normal force F_n. With the progress of the tool's flank wear, the main angle κ_r increases, which made the feed force F_x more sensitive to the tool's flank wear than the axial force F_z. Finally, we also found that the recognition accuracy was obviously improved by integrating data from three sensors in different directions via CHMM_*r*. The reason for this could be the fact that each chain in the CHMM_*r* was used to describe the statistical properties of the data acquired by a sensor in a single direction, and then, the three chains were combined on basis of the conditional probability of the coupling states in the three directions. Therefore, the tool wear state could be more comprehensively described by fusing the data of the sensors in the three directions, which enabled CHMM_*r* to preserve the advantages of HMMs.

B. APPLICATION TO SURFACE ROUGHNESS ACCURACY GRADE PREDICTION

1) MATERIAL AND EQUIPMENT

The turning tests were conducted using a lathe CK6140 under dry conditions at the Engineering Training Center, Southeast University, Nanjing, China. The cutting tool used was a Japan Sumitomo BNC160, and a workpiece with multiple materials and hardness scales was adopted. In view of the advantages of the cutting vibration for the surface quality monitoring [3], [4], three acceleration sensors PCB 608A11 were placed close to the tool tip to measure the cutting vibrations. The signals of the three accelerometers were acquired and processed by means of a 24-bit multichannel A/D analysis test system TST5915, which was connected to a laptop running the MATLAB 7.8 software. The sampling rate was $f_s = 20\,k$Hz. The experimental setup is shown in FIGURE 12.

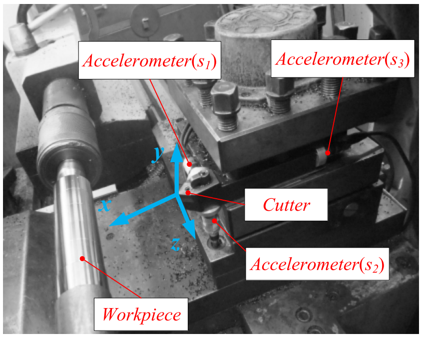

FIGURE 12. **CNC turning machine testbed.**

According to the accuracy grade of the arithmetic mean deviation (*Ra*) defined by GB/T1031-2009, the surface roughness Ra obtained in the experiment was divided into three levels: accuracy grade 9(*G9*), *G9* $\leq$ *Ra0.4*; accuracy grade 8(*G8*), *Ra0.4* < *G8* $\leq$ *Ra0.8*, and accuracy grade 7(*G7*), *Ra0.8* < *G7* $\leq$ *Ra1.6*. To extract the robust and efficient features and analyze the effect of the sensor layout on the accuracy of the system, the feature E_R was extracted from the vibration signal picked up by sensors s_1, s_2, and s_3, and then, was encoded using a 4 × 4 codebook based on SOM. To further optimize the feature, the second-order feature selection method discussed above was adopted for the feature selection. TABLE 5 shows the cutting parameters, feature selected, code, and the corresponding surface roughness.

By using the encoding obtained from SOM, the observation symbol probability distribution is estimated based on the Baum-Welch algorithm. According to experience, the structural parameters of each model are selected, as shown in TABLE 6.

For the HMM, both the initial state probability vector π and the state transition probability matrix $\boldsymbol{A}$ were uniformly initialized, and the observation symbol probability matrix $\boldsymbol{B}$ was estimated according to Eq. (14). For example, the π and $\boldsymbol{A}$ of the HMM were uniformly initialized as follows:

$$\pi = \begin{bmatrix} \frac{1}{3} \\ \frac{1}{3} \\ \frac{1}{3} \end{bmatrix}, \quad A = \begin{bmatrix} \frac{1}{3} & \frac{1}{3} & \frac{1}{3} \\ \frac{1}{3} & \frac{1}{3} & \frac{1}{3} \\ \frac{1}{3} & \frac{1}{3} & \frac{1}{3} \end{bmatrix}$$

TABLE 5. Experimental parameters and results obtained.

No.	Workpiece properties		Cutting variables			Response variables						
	Material	Hardness (HRC)	*Vc* (*m/min*)	*f* (*mm/r*)	*ap* (*mm*)	E_R			*Code*			*Ra* (μm)
						s_1	s_2	s_3	c_1	c_2	c_3	
1	AISI4340	55	180	0.12	0.2	0.499	0.457	0.592	9	10	9	0.471
2	AISI4340	50	180	0.18	0.1	0.157	0.454	0.480	8	10	9	0.586
3	AISI4340	55	140	0.03	0.1	0.289	0.216	0.091	7	12	16	0.611
4	AISI4340	55	140	0.03	0.2	0.274	0.330	0.013	11	6	16	0.698
5	AISID2	55	100	0.03	0.3	0.476	0.445	0.488	9	9	9	0.834
6	AISID2	60	100	0.03	0.2	0.472	0.549	0.455	9	9	6	0.908
7	ASTM1045	30	84	0.12	1	0.258	0.358	0.172	10	5	7	0.655
8	ASTM1045	30	60	0.09	1	0.025	0.287	0.063	16	10	16	0.876
9	ASTM1045	30	60	0.12	1.2	0.141	0.230	0.056	12	11	16	0.991
10	AISID2	55	100	0.21	0.1	0.017	0.463	0.454	16	9	9	0.873
11	AISI4340	50	180	0.21	0.3	0.493	0.410	0.655	9	5	9	0.750
12	AISI4340	50	180	0.21	0.1	0.457	0.414	0.139	10	11	8	1.019
13	AISI4340	50	180	0.04	0.1	0.419	0.040	0.099	11	8	8	0.977
14	AISI4340	55	140	0.1	0.2	0.489	0.467	0.367	1	1	2	0.366
15	AISI4340	55	140	0.12	0.3	0.329	0.334	0.358	6	6	2	0.373
16	AISID2	60	100	0.12	0.2	0.001	0.305	0.021	16	15	7	0.467
17	AISID2	55	100	0.21	0.3	0.045	0.417	0.174	16	10	15	0.537
18	ASTM1045	30	60	0.12	0.6	0.002	0.244	0.039	16	11	16	1.172
19	AISI4340	50	180	0.03	0.2	0.493	0.435	0.488	9	11	9	0.675
20	AISI4340	55	140	0.21	0.1	0.346	0.366	0.231	6	2	11	0.526
21	AISID2	55	100	0.18	0.1	0.014	0.392	0.351	16	10	16	0.618
22	ASTM1045	30	131	0.12	1	0.248	0.479	0.320	10	1	5	0.561
23	AISI4340	50	180	0.12	0.3	0.489	0.447	0.473	9	14	13	0.496
24	AISI4340	55	180	0.03	0.1	0.477	0.449	0.479	9	14	9	0.611
25	AISI4340	50	140	0.21	0.3	0.295	0.111	0.272	7	15	11	0.528
26	AISI4340	55	140	0.21	0.2	0.309	0.019	0.237	7	16	11	0.551
27	AISID2	60	100	0.21	0.2	0.013	0.404	0.160	16	10	15	0.576
28	AISID2	55	100	0.12	0.1	0.007	0.277	0.247	16	11	7	0.705
29	ASTM1045	30	60	0.12	0.3	0.236	0.376	0.394	11	1	1	0.759
30	ASTM1045	30	60	0.12	1.5	0.218	0.229	0.045	7	10	16	0.846
31	AISI4340	55	180	0.2	0.2	0.010	0.452	0.469	8	10	13	0.701
32	AISI4340	50	180	0.03	0.3	0.456	0.443	0.486	10	14	9	0.651
33	ASTM1045	30	60	0.12	1	0.144	0.239	0.045	12	5	16	1.119
34	ASTM1045	30	60	0.12	0.9	0.216	0.238	0.055	7	11	16	1.157
35	AISI4340	50	140	0.2	0.3	0.350	0.005	0.091	3	16	6	0.689
36	AISI4340	55	140	0.03	0.3	0.308	0.081	0.330	7	16	16	0.793
37	AISI4340	50	180	0.21	0.2	0.450	0.346	0.310	14	12	12	1.081
38	AISID2	60	100	0.2	0.3	0.493	0.487	0.453	9	9	9	0.835
39	AISID2	60	100	0.04	0.1	0.012	0.610	0.496	16	9	9	0.887
40	ASTM1045	30	60	0.12	1.8	0.101	0.212	0.106	15	10	15	0.901
41	ASTM1045	30	60	0.06	1	0.165	0.330	0.041	8	2	16	1.211
42	AISI4340	55	140	0.04	0.1	0.426	0.553	0.013	1	1	3	0.283
43	AISI4340	55	140	0.14	0.3	0.485	0.468	0.045	1	1	2	0.397
44	AISID2	55	100	0.14	0.2	0.009	0.139	0.240	16	15	7	0.515
45	AISID2	60	100	0.12	0.3	0.001	0.403	0.206	16	10	4	0.457
46	ASTM1045	30	107	0.12	1	0.367	0.401	0.281	1	1	16	0.624
47	AISID2	60	100	0.03	0.1	0.465	0.526	0.462	9	9	9	0.813
48	ASTM1045	30	155	0.12	1	0.227	0.464	0.183	11	1	7	0.540

when training two or three chains coupled to CHMM_w or CHMM_r, $\boldsymbol{\pi}$ and $\boldsymbol{A}$ were uniformly initialized. For the $\boldsymbol{B}$ parameters, each chain of CHMM was initialized individually by the method conducted in HMM, and then, the initial results of each chain were regarded as the initial value of $\boldsymbol{B}$.

TABLE 6. Model structure parameters.

Model	Axis	Sensor	Model structure		
			Markov chain type	Number of states	Inference engine
HMM	y	s_2	Ergodic	3	Forward-Backward Algorithm
	x	s_3	Ergodic	3	Forward-Backward Algorithm
	z	s_1	Ergodic	3	Forward-Backward Algorithm
CHMM_w	y, x	s_2,s_3	Ergodic	3×3	jtree_dbn
	y, z	s_2,s_1	Ergodic	3×3	jtree_dbn
	x, z	s_1,s_3	Ergodic	3×3	jtree_dbn
CHMM_r	x, y, z	s_1,s_2,s_3	Ergodic	3×3×3	jtree_dbn

2) RESULTS AND DISCUSSION

Based on the features selected, the data in TABLE 5 (rows 1 to 22) were used as the training sets for model building. The EM algorithm discussed above was used for λ_{G9}, λ_{G8}, and λ_{G7} learning. To analyze the effect of the senor layout on the accuracy of the model, the data picked up by a single sensor in one direction, two sensors in two directions, and three sensors in three directions were adopted to train HMM, CHMM_w, and CHMM_r, respectively. Then, the data in TABLE 5 (rows 23 to 48) were used for the model testing. The corresponding results are shown in FIGURES 13∼15. As shown in FIGURE 15, the data coupling of the s_1, s_2, and s_3 sensors more comprehensively reflected the effect of tool vibration on the surface topography, and thus, we concluded that CHMM_$r$could identify the Ra accuracy grade in the turning process accurately.

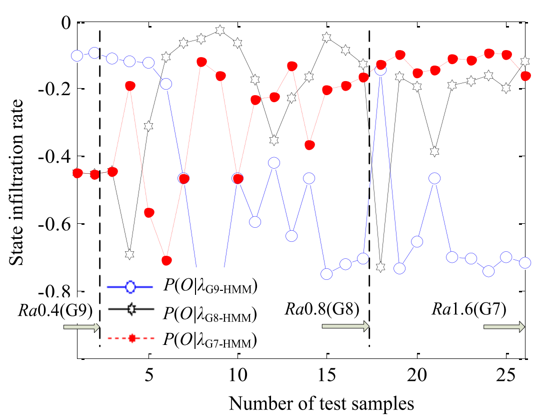

FIGURE 13. SIR of HMM using the s_2 sensor.

To quantify the effect of sensor deployment on the accuracy of the system, the results defined by Eq. (16) are summarized in TABLE 7. When a single sensor was used, for example, {s_1}, {s_2}, or {s_3}, the recognition rate of the HMMs was relatively low. As a result of the analysis discussed above,

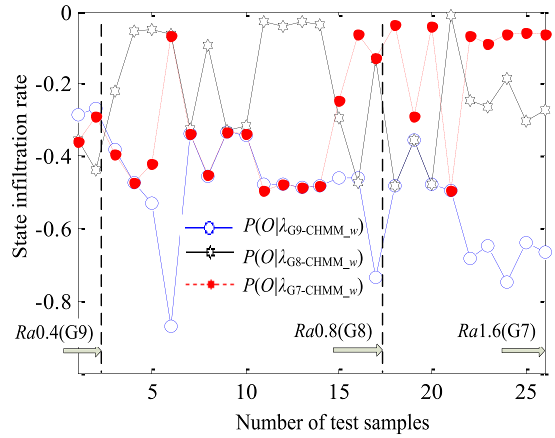

FIGURE 14. SIR of CHMM_w using the s_1 and s_3 sensors.

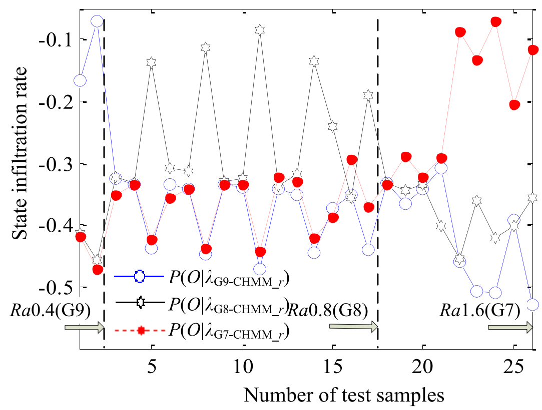

FIGURE 15. SIR of CHMM_r using the s_1, s_2, and s_3 sensors.

TABLE 7. Identified results using different sensor layouts.

Approach	Orientation	Sensor layout	Sample size	C_R
HMM	y dir.	{s_2}	26	77%
	x dir.	{s_3}	26	73%
	z dir.	{s_1}	26	73%
CHMM_w	y dir., x dir.	{s_2,s_3}	26	58%
	y dir., z dir.	{s_2,s_1}	26	81%
	x dir., z dir.	{s_1,s_3}	26	85%
CHMM_r	x dir. y dir. z dir.	{s_1,s_2,s_3}	26	89%

the vibration signal in a single direction could not provide the complete information of surface topography, and therefore, the CHMM_w with the data fusion of two sensors preserved the advantages of the HMMs. However, for the sensor layout {s_2, s_3}, the recognition rate using CHMM_w was lower than that obtained using HMMs. The reason for this difference was as follows: Sensors s_2 and s_3, respectively, picked up the tool vibration signals in the tangential (y) and radial (x) directions, as shown in FIGURE 2. During the turning process, the change in the depth of cut (x) was largely dependent on the offset of the tool vibration in the tangential direction, in which the change in the amplitude altered the depth of cut [39]. Moreover, the depth of cut was affected by the effect of the workpiece on the tool tip along the radial direction. Both of these factors led to changes in the depth of cut. However, these two vibration effects on the cutting depth were not fully synchronized (e.g., the effect occurred only when there was a contact). Therefore, the data fusion of sensors s_2 and s_3 was bound to cause more interference, which led to the lower recognition rate using CHMM_w than that obtained using HMMs. Compared with HMMs and CHMM_w, CHMM_r took advantage of the surface topography information fully described by sensors $\{s_1, s_2, s_3\}$, resulting in a more accurate prediction.

V. CONCLUSION

In the aircraft and automotive industries, the successful application of manufacturing process automation hinges primarily on the effectiveness of the process monitoring. This paper discussed the monitoring of a machining process by using multi-directional data fusion based on DBNs and analyzed the effect of the sensor layout on the monitoring accuracy. The empirical study had the following outcomes:

(1) The tool wear process or the formation of the workpiece surface topography had considerable uncertainty and randomness. Therefore, the stochastic model-DBN-based approach, CHMM proposed in this paper, could be well used for supervising the machining process. This approach was tested and validated successfully in the tool wear and surface roughness prediction cases. For the tool wear case, CHMM_r detected correctly the tool wear state (i.e., *IS*, *GS*, or *AS*) with a success rate of 89%. Further, in the surface roughness accuracy prediction tests, the success rate obtained during testing was 89%. Which further broadening and making up for the inadequacy of BN in the field of condition monitoring in machining process

(2) The feature extraction strategy, based on the singular spectrum and wavelet analysis, could be well used to extract the features required for the monitoring of a machining process. The two case studies, i.e., tool wear in a high-speed milling process and surface roughness prediction under the multiple materials and hardness scale conditions in the turning process, showed that this feature extraction method had some versatility in feature extraction for supervising the machining process. Which provides a new tool and strategy for feature extraction in wavelet domain.

(3) In the monitoring of a machining process, sensor deployment had a significant effect on the monitoring precision. In the high-speed milling case, when a unidirectional sensor S_z (z dir.), S_y (y dir.), or S_x (x dir.) was selected, the tool wear state recognition rate calculated using HMMs was 50%, 75%, and 83%, respectively. In contrast, when the triaxial sensors were selected, the tool wear state recognition rate obtained using CHMM_r was 89%. In the case of turning the workpiece with multiple materials and hardness scales, when we selected a single sensor s_1 (axial), s_3 (radial), or s_2 (tangential) for the arrangement, the recognition rate of the Ra accuracy grade prediction using HMMs was 73%, 73%, and 77%, respectively. When two sensors $\{s_2, s_3\}$, $\{s_2, s_1\}$, or $\{s_1, s_3\}$ were deployed, the recognition rate of obtained using CHMM_w was 58%, 81%, and 85%, respectively. In contrast, in the three-sensor layout, the recognition rate obtained using CHMM_r was 89%. Therefore, different sensor arrangements can be selected to meet a variety of accuracy requirements for the monitoring of a machining process.

The DBN-based methodology proposed for machining process monitoring still has its limitations. With the increase in number of sensing points, sensing data acquisition and feature selection are laborious and susceptible to human error. Moreover, fewer sensing points make it impossible to effectively optimize the sensor network based on the DBN-based fusion results. Future work will investigate the automatic data acquisition and feature selection techniques, as well as the multi-sensor optimization placement strategy using DBN-based state recognition method.

REFERENCES

[1] A. Caggiano, "Cloud-based manufacturing process monitoring for smart diagnosis services," *Int. J. Comput. Integr. Manuf.*, vol. 31, no. 7, pp. 612–623, 2018.

[2] R. S. U. Raju, R. Ramesh, V. R. Raju, and S. Mohammad, "Curvelet transforms and flower pollination algorithm based machine vision system for roughness estimation," *J. Opt.*, vol. 47, no. 2, pp. 243–250, Jun. 2018.

[3] N. Xie, J. Zhou, and B. Zheng, "An energy-based modeling and prediction approach for surface roughness in turning," *Int. J. Adv. Manuf. Technol.*, vol. 96, nos. 5–8, pp. 2293–2306, 2018.

[4] Z. Ge, Z. Song, and F. Gao, "Review of recent research on data-based process monitoring," *Ind. Eng. Chem. Res.*, vol. 52, no. 10, pp. 3543–3562, 2013.

[5] K. V. Rao and P. B. G. S. N. Murthy, "Modeling and optimization of tool vibration and surface roughness in boring of steel using RSM, ANN and SVM," *J. Intell. Manuf.*, pp. 1–11, Jan. 2016.

[6] I. Belakhdar, W. Kaaniche, R. Djmel, and B. Ouni, "A comparison between ANN and SVM classifier for drowsiness detection based on single EEG channel," in *Proc. 2nd Int. Conf. ATSIP*, Monastir, Tunisia, Mar. 2016, pp. 443–446.

[7] T. Zhou, F. Wang, and Z. Yang, "Comparative analysis of ANN and SVM models combined with wavelet preprocess for groundwater depth prediction," *Water*, vol. 9, no. 10, p. 781, 2017.

[8] Z. Ge, Z. Song, S. X. Ding, and B. Huang, "Data mining and analytics in the process industry: The role of machine learning," *IEEE Access*, vol. 5, pp. 20590–20616, 2017.

[9] J. Liu, Y. Hu, Y. Wang, B. Wu, J. Fan, and Z. Hu, "An integrated multi-sensor fusion-based deep feature learning approach for rotating machinery diagnosis," *Meas. Sci. Technol.*, vol. 29, no. 5, p. 055103, 2018.

[10] C. Lu, "Study on prediction of surface quality in machining process," *J. Mater. Process. Technol.*, vol. 205, nos. 1–3, pp. 439–450, Aug. 2008.

[11] K. Patra, A. K. Jha, T. Szalay, J. Ranjan, and L. Monostori, "Artificial neural network based tool condition monitoring in micro mechanical peck drilling using thrust force signals," *Precis. Eng.*, vol. 48, pp. 279–291, Apr. 2017.

[12] S. Karagiannis, P. Stavropoulos, C. Ziogas, and J. Kechagias, "Prediction of surface roughness magnitude in computer numerical controlled end milling processes using neural networks, by considering a set of influence parameters: An aluminium alloy 5083 case study," *Proc. Inst. Mech. Eng., B, J. Eng. Manuf.*, vol. 228, no. 2, pp. 233–244, Feb. 2014.

[13] I. Asiltürk and M. Çunkaş, "Modeling and prediction of surface roughness in turning operations using artificial neural network and multiple regression method," *Expert Syst. Appl.*, vol. 38, no. 5, pp. 5826–5832, 2011.

[14] D. Lipiński, B. Bałasz, and Ł. Rypina, "Modelling of surface roughness and grinding forces using artificial neural networks with assessment of the ability to data generalisation," *Int. J. Adv. Manuf. Technol.*, vol. 94, nos. 1–4, pp. 1335–1347, Jan. 2018.
[15] Z. Ge, "Review on data-driven modeling and monitoring for plant-wide industrial processes," *Chemometrics Intell. Lab. Syst.*, vol. 171, pp. 16–25, Dec. 2017.
[16] T. Boutros and M. Liang, "Detection and diagnosis of bearing and cutting tool faults using hidden Markov models," *Mech. Syst. Signal Process.*, vol. 25, no. 6, pp. 2102–2124, 2011.
[17] M. Correa, C. Bielza, and J. Pamies-Teixeira, "Comparison of Bayesian networks and artificial neural networks for quality detection in a machining process," *Expert Syst. Appl.*, vol. 36, no. 3, pp. 7270–7279, Apr. 2009.
[18] J. Zhu, Z. Ge, Z. Song, L. Zhou, and G. Chen, "Large-scale plant-wide process modeling and hierarchical monitoring: A distributed Bayesian network approach," *J. Process. Control*, vol. 65, pp. 91–106, May 2018.
[19] Z. Liu, Z. Ge, G. Chen, and Z. Song, "Adaptive soft sensors for quality prediction under the framework of Bayesian network," *Control Eng. Pract.*, vol. 72, pp. 19–28, Mar. 2018.
[20] D. A. Tobon-Mejia, K. Medjaher, and N. Zerhouni, "CNC machine tool's wear diagnostic and prognostic by using dynamic Bayesian networks," *Mech. Syst. Signal Process.*, vol. 28, pp. 167–182, Apr. 2012.
[21] S. Mandal, V. K. Sharma, A. Pal, and Nagahanumaiah, "Tool strain–based wear estimation in micro turning using Bayesian networks," *Proc. Inst. Mech. Eng., B, J. Eng. Manuf.*, vol. 230, no. 10, pp. 1952–1960, 2016.
[22] J. V. A. Nebot, R. Morales-Menéndez, A. J. V. Guevara, and C. A. Rodríguez, "Surface roughness and cutting tool-wear diagnosis based on Bayesian networks," in *Proc. Conf. FDSSTP*, 2006, pp. 408–413.
[23] J. Karandikar, T. Mcleay, S. Turner, and T. Schmitz, "Tool wear monitoring using naive Bayes classifiers," *Int. J. Adv. Manuf. Technol.*, vol. 77, nos. 9–12, pp. 1613–1626, 2015.
[24] D. McParland, S. Baron, S. O'Rourke, D. Dowling, E. Ahearne, and A. Parnell, "Prediction of tool-wear in turning of medical grade cobalt chromium molybdenum alloy (ASTM F75) using non-parametric Bayesian models," *J. Intell. Manuf.*, pp. 1–12, Mar. 2017.
[25] A. Al-Habaibeh and N. Gindy, "A new approach for systematic design of condition monitoring systems for milling processes," *J. Mater. Process. Technol.*, vol. 107, nos. 1–3, pp. 243–251, Nov. 2000.
[26] T.-I. Liu, S.-D. Song, G. Liu, and Z. Wu, "Online monitoring and measurements of tool wear for precision turning of stainless steel parts," *Int. J. Adv. Manuf. Technol.*, vol. 65, nos. 9–12, pp. 1397–1407, 2013.
[27] H. Saglam, "Tool wear monitoring in bandsawing using neural networks and Taguchi's design of experiments," *Int. J. Adv. Manuf. Technol.*, vol. 55, nos. 9–12, pp. 969–982, 2011.
[28] D. M. D'Addona, A. M. M. S. Ullah, and D. Matarazzo, "Tool-wear prediction and pattern-recognition using artificial neural network and DNA-based computing," *J. Intell. Manuf.*, vol. 28, no. 6, pp. 1285–1301, 2017.
[29] D. Rajeev, D. Dinakaran, and S. C. E. Singh, "Artificial neural network based tool wear estimation on dry hard turning processes of AISI4140 steel using coated carbide tool," *Bull. Polish Acad. Sci. Tech. Sci.*, vol. 65, no. 4, pp. 553–559, 2017.
[30] A. Salimiasl, A. Erdem, and M. Rafighi, "Applying a multi-sensor system to predict and simulate the tool wear using artificial neural networks," *Sci. Iranica Trans. B, Mech. Eng.*, vol. 24, no. 6, pp. 2864–2874, Nov. 2017.
[31] P. S. Paul and A. S. Varadarajan, "ANN assisted sensor fusion model to predict tool wear during hard turning with minimal fluid application," *Int. J. Mach. Machinab. Mater.*, vol. 13, no. 4, pp. 398–413, 2013.
[32] M. Elgargni, A. Al-Habaibeh, and A. Lotfi, "Cutting tool tracking and recognition based on infrared and visual imaging systems using principal component analysis (PCA) and discrete wavelet transform (DWT) combined with neural networks," *Int. J. Adv. Manuf. Technol.*, vol. 77, nos. 9–12, pp. 1965–1978, 2015.
[33] M. N. Khajavi, E. Nasernia, and M. Rostaghi, "Milling tool wear diagnosis by feed motor current signal using an artificial neural network," *J. Mech. Sci. Technol.*, vol. 30, no. 11, pp. 4869–4875, 2016.
[34] K. V. Rao, K. P. Vidhu, T. A. Kumar, N. N. Rao, P. B. G. S. N. Murthy, and M. Balaji, "An artificial neural network approach to investigate surface roughness and vibration of workpiece in boring of AISI1040 steels," *Int. J. Adv. Manuf. Technol.*, vol. 83, nos. 5–8, pp. 919–927, 2016.
[35] I. Maher, M. E. H. Eltaib, A. A. D. Sarhan, and R. M. El-Zahry, "Cutting force-based adaptive neuro-fuzzy approach for accurate surface roughness prediction in end milling operation for intelligent machining," *Int. J. Adv. Manuf. Technol.*, vol. 76, nos. 5–8, pp. 1459–1467, 2015.
[36] G. Quintana, T. Rudolf, J. Ciurana, and C. Brecher, "Surface roughness prediction through internal kernel information and external accelerometers using artificial neural networks," *J. Mech. Sci. Technol.*, vol. 25, no. 11, pp. 2877–2886, 2011.
[37] S. Palani and U. Natarajan, "Prediction of surface roughness in CNC end milling by machine vision system using artificial neural network based on 2D Fourier transform," *Int. J. Adv. Manuf. Technol.*, vol. 54, nos. 9–12, pp. 1033–1042, 2011.
[38] A. M. Khorasani and M. R. S. Yazdi, "Development of a dynamic surface roughness monitoring system based on artificial neural networks (ANN) in milling operation," *Int. J. Adv. Manuf. Technol.*, vol. 93, nos. 1–4, pp. 141–151, 2017.
[39] I. Asilturk, H. Kahramanli, and H. El Mounayri, "Prediction of cutting forces and surface roughness using artificial neural network (ANN) and support vector regression (SVR) in turning 4140 steel," *J. Mater. Sci. Technol.*, vol. 28, no. 8, pp. 980–986, 2012.
[40] R. E. Haber, J. E. Jiménez, C. R. Peres, and J. R. Alique, "An investigation of tool-wear monitoring in a high-speed machining process," *Sens. Actuators A, Phys.*, vol. 116, no. 3, pp. 539–545, 2004.
[41] M. Wiciak, P. Twardowski, and S. Wojciechowski, "Comparison of various tool wear prediction methods during end milling of metal matrix composite," *Arch. Mech. Technol. Meter.*, vol. 38, no. 1, pp. 1–7, 2018.
[42] S.-L. Chen and Y. W. Jen, "Data fusion neural network for tool condition monitoring in CNC milling machining," *Int. J. Mach. Tools Manuf.*, vol. 40, no. 3, pp. 381–400, Feb. 2000.
[43] T. Prasetyo, S. Amar, A. Arendra, and M. K. Z. Zami, "On-line tool wear detection on DCMT070204 carbide tool tip based on noise cutting audio signal using artificial neural network," *J. Phys., Conf. Ser.*, vol. 953, no. 1, p. 012144, 2018.
[44] T.-I. Liu and B. Jolley, "Tool condition monitoring (TCM) using neural networks," *Int. J. Adv. Manuf. Technol.*, vol. 78, nos. 9–12, pp. 1999–2007, 2015.
[45] N. Fang, N. Fang, P. S. Pai, and N. Edwards, "Neural network modeling and prediction of surface roughness in machining aluminum alloys," *J. Comput. Commun.*, vol. 4, no. 5, pp. 1–9, 2017.
[46] N. Ghosh *et al.*, "Estimation of tool wear during CNC milling using neural network-based sensor fusion," *Mech. Syst. Signal Process.*, vol. 21, no. 1, pp. 466–479, Jan. 2007.
[47] X. Yang, "Wear state recognition of drills based on K-means cluster and radial basis function neural network," *Int. J. Automat. Comput.*, vol. 7, no. 3, pp. 271–276, 2010.
[48] J. V. Abellan-Nebot and F. R. Subirón, "A review of machining monitoring systems based on artificial intelligence process models," *Int. J. Adv. Manuf. Technol.*, vol. 47, nos. 1–4, pp. 237–257, 2010.
[49] J. H. Oh and S. H. Lee, "Prediction of surface roughness in magnetic abrasive finishing using acoustic emission and force sensor data fusion," *Proc. Inst. Mech. Eng., B, J. Eng. Manuf.*, vol. 225, no. 6, pp. 853–865, 2011.
[50] K. He, Q. Xu, and M. Jia, "Modeling and predicting surface roughness in hard turning using a Bayesian inference-based HMM-SVM model," *IEEE Trans. Autom. Sci. Eng.*, vol. 12, no. 3, pp. 1092–1103, Jul. 2015.
[51] J. G. A. Arulraj, K. L. D. Wins, and A. Raj, "Artificial neural network assisted sensor fusion model for predicting surface roughness during hard turning of H13 steel with minimal cutting fluid application," *Procedia Mater. Sci.*, vol. 5, no. 5, pp. 2338–2346, 2014.
[52] K. Zhu, W. Y. San, and G. S. Hong, "Wavelet analysis of sensor signals for tool condition monitoring: A review and some new results," *Int. J. Mach. Tools Manuf.*, vol. 49, nos. 7–8, pp. 537–553, Jun. 2009.
[53] H. Wang, S. To, C. Y. Chan, C. F. Cheung, and W. B. Lee, "A theoretical and experimental investigation of the tool-tip vibration and its influence upon surface generation in single-point diamond turning," *Int. J. Mach. Tools Manuf.*, vol. 50, no. 3, pp. 241–252, Mar. 2010.
[54] H. Ghorbani and B. Moetakef-Imani, "Specific cutting force and cutting condition interaction modeling for round insert face milling operation," *Int. J. Adv. Manuf. Technol.*, vol. 84, nos. 5–8, pp. 1705–1715, 2016.
[55] H. Zhao, G. C. Barber, and Q. Zou, "A study of flank wear in orthogonal cutting with internal cooling," *Wear*, vol. 253, nos. 9–10, pp. 957–962, Nov. 2002.
[56] Y. Mei, R. Mo, H. Sun, and K. Bu, "Chatter detection in milling based on singular spectrum analysis," *Int. J. Adv. Manuf. Technol.*, vol. 95, nos. 9–12, pp. 3475–3486, 2018.
[57] J.-R. Chazottes, P. Collet, and F. Redig, "On concentration inequalities and their applications for Gibbs measures in lattice systems," *J. Stat. Phys.*, vol. 169, no. 3, pp. 504–546, 2017.

[58] X. Zhang, S. Ding, and T. Sun, "Multi-class LSTMSVM based on optimal directed acyclic graph and shuffled frog leaping algorithm," *Int. J. Mach. Learn. Cybern.*, vol. 7, no. 2, pp. 241–251, 2016.
[59] Y.-S. Hong, H.-S. Yoon, J.-S. Moon, Y.-M. Cho, and S.-H. Ahn, "Tool-wear monitoring during micro-end milling using wavelet packet transform and Fisher's linear discriminant," *Int. J. Precis. Eng. Manuf.*, vol. 17, no. 7, pp. 845–855, 2016.
[60] PHM Society. (2010). *PHM Data Challenge*. [Online]. Available: https://www.Phmsociety.org/competition/phm/10S

KANG HE received the B.S. degree in mechanical engineering from the Henan University of Science and Technology, Luoyang, China, in 2003, the M.S. degree in mechanical engineering from Nanchang University, Nanchang, China, in 2010, and the Ph.D. degree in mechanical engineering from Southeast University, Nanjing, China, in 2015.

From 2004 to 2007, he served as a Green Belt for the machining of automobile engine in Engine plant of Jiangling Motors Corporation, Ltd. (The joint ventures with Ford?, Nanchang, China. From 2011 to 2012, he was responsible for the engine assembly as a Principal Engineer in Engine plant of Jiangling Motors Corporation, Ltd. During this period, he was responsible for the completion of the ?14 twist drill performance improvement projects, ?28 oil pump orifice reamer quality improvement projects, and annual savings of processing costs 120,000 Yuan. He has published over 10 academic papers, including the IEEE Transactions on Automation Science & Engineering, the *Journal of Mechanical Engineering*(in chinese), and the *International Journal of Advanced Manufacturing Technology*.

Dr. He is currently an Assistant Professor of electromechanical engineering, a Key Member of Mine Machinery and Electronic Engineering Research Center, and a public bidding evaluation expert with Suzhou University. His current research interests include fault diagnosis, manufacturing process condition monitoring, and quality assurance. He currently serves as the reviewer for several journals.

ZHUANZHE ZHAO received the B.S. degree in mechanical manufacture and automation and the M.S. degree in measuring and testing technologies and instruments from the Henan University of Science and Technology, Luoyang, China, in 2002 and 2005, respectively, and the Ph.D. degree in mechanical manufacture and automation from Southeast University, Nanjing, China, in 2016.

He is currently an Associate Professor and a member of the Key Laboratory of Advanced Numerical Control and Servo Drive Technology of Anhui Province with Anhui Polytechnic University. His current research interests include the intelligent computing, mechanical condition monitoring, and fault diagnosis. Dr. Zhao is currently a Key Member of the Key Laboratory of Advanced Numerical Control and Servo Drive Technology of Anhui Province. He has published over 10 academic papers, including *Neural Computing and Application* and *Nat Comput*. He has been invited to be a reviewer for several SCI/EI journals.

MINPING JIA received the B.S. and M.S. degrees in mechanical engineering from the Nanjing Institute of Technology (now Southeast University), Nanjing, China, in 1982 and 1985, respectively, and the Ph.D. degree in mechanical engineering from Southeast University, Nanjing, China, in 1991. He is currently a Full Professor with Southeast University. His research interests include the intelligent computing, dynamic signal processing, machine fault diagnosis, and vibration engineering applications.

Dr. Jia is the Director of the China Society for Vibration Engineering, an Associate Director of the Professional Technical Committee on Dynamic Signal Analysis, and a member of the Test Technology Committee of Chinese Production Engineering Institution. He received three times of Science and Technology Progress Awards from the Ministry of Education of China and Jiangsu Province. He serves as an Associate Editor of the *Journal of Vibration Engineering*.

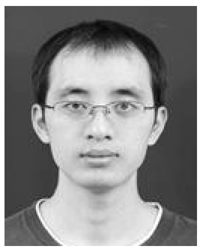

CONGHU LIU received the B.S. degree in industrial engineering from Henan Polytechnic University, Jiaozuo City, China, in 2005, the M.S. degree in mechanical engineering from Chongqing University, Chongqing, China, in 2009, and the Ph.D. degree in mechanical engineering from the Hefei University of Technology, Hefei, China, in 2016.

From 2009 to 2015, he was a Teacher in mechanical engineering with Anhui Polytechnic University, and since 2016, he has been doing Post-Doctoral Studies with Shanghai Jiao Tong University. His research directions are green manufacturing and sustainable supply chain. Dr. Liu currently a Post-Doctoral Researcher with the Sino-US Global Logistics Institute, Shanghai Jiao Tong University. He has published over 10 academic papers, including *Energy*, *Journal of Cleaner Production*,*Assembly Automation*, and *The International Journal of Advanced Manufacturing Technology*. He has been invited to be a reviewer for several SCI/EI journals.